American Mineralogist, Volume 77, pages 937–944, 1992

High-pressure crystal chemistry of cubanite, $CuFe_2S_3$

CATHERINE MCCAMMON,* JINMIN ZHANG, ROBERT M. HAZEN, LARRY W. FINGER
Geophysical Laboratory and Center for High-Pressure Research, Carnegie Institution of Washington, 5251 Broad Branch Road NW, Washington, DC 20015-1305, U.S.A.

ABSTRACT

We have studied cubanite, $CuFe_2S_3$ (orthorhombic, space group *Pcmn*, $a = 6.46$, $b = 11.10$, $c = 6.22$ Å), using single-crystal X-ray diffraction in a diamond-anvil cell at room temperature from 0 to 3.68 GPa. Refinements were performed at 0, 1.76, and 3.59 GPa, and cell parameters were measured at 20 pressures up to 3.68 GPa. The linear compressibilities of the *a*, *b*, and *c* crystal axes are 0.00513(5), 0.00479(5), and 0.00575(4) GPa^{-1}, respectively. Compressibility data were fitted to a Birch-Murnaghan equation of state with parameters $K_0 = 55.3 \pm 1.7$ GPa with K_0' constrained to be 4. High-pressure refinement data indicate that the principal response of the crystal structure to compression is a reduction in Cu-S bond lengths, whereas Fe-S bond lengths remain essentially unchanged. Results are compared to bulk moduli and polyhedral bulk moduli of other sulfides.

INTRODUCTION

The crystal structure of cubanite, $CuFe_2S_3$, is orthorhombic with ordered tetrahedral cation sites and S atoms in approximately hexagonal closest packing. The structure was first determined by Buerger (1945, 1947) and described as slices of wurtzite structure parallel to (010) with width $b/2$, joined such that every other slab is inverted, resulting in edge-shared pairs of tetrahedra. The valence of Cu has been established as +1 on the basis of neutron diffraction data (Wintenberger et al., 1974), whereas Fe atoms appear to occupy adjacent edge-shared tetrahedra as Fe^{2+} and Fe^{3+}, with rapid electron exchange between them. Crystal structure refinements indicate centrosymmetric space group *Pcmn*, which implies that the two Fe atoms are in identical oxidation states across the center of symmetry on a time-averaged basis (Fleet, 1970; Szymanski, 1974). Mössbauer spectra show only one site for Fe from 4.2 K to room temperature (Imbert and Wintenberger, 1967; Greenwood and Whitfield, 1968), which is consistent with Fe atoms in the same valence state on the time scale of the Mössbauer effect (1.5×10^{-7} s). From neutron diffraction data, Wintenberger et al. (1974) found a single Fe moment of 3.2 μ_B, consistent with rapid electron exchange. Electrical resistivity data of Sleight and Gillson (1973) have shown that cubanite is a semiconductor, implying that rapid electron exchange is confined to pairs of edge-shared tetrahedra.

Goodenough (1980) has shown that the edge-shared configuration of Fe tetrahedra should stabilize the Fe^{2+}-Fe^{3+} configuration. An interesting problem, therefore, is the effect of pressure on electron transfer, since the crystal structure will inevitably change. High-pressure crystallography provides an excellent means for examining the effect of pressure on individual atomic configurations. Cubanite is a worthy candidate because of the interest in the effect of pressure on intervalence transitions (see, for example, Burns, 1981) and because very few sulfides have been examined with this technique. We undertook a crystallographic study of cubanite at high pressure with the following goals: (1) to determine the relative axial compressibilities and bulk modulus of cubanite, (2) to observe changes in cation-anion configurations with pressure through variations in bond lengths, bond angles, and tetrahedral geometries, and (3) to examine the effect of pressure on the electron structure of Fe, based on changes in the atomic arrangements.

EXPERIMENTAL METHODS

Room conditions experiment

A single crystal of cubanite was selected from sample R17907 (Morro Velho, Nova Lima, Brazil) provided by the National Museum of Natural History, Smithsonian Institution, Washington, DC. A rectangular prismatic cleavage fragment, approximately $30 \times 60 \times 100$ μm, was used for the X-ray diffraction experiments. Data on a crystal mounted in air were obtained with a Rigaku AFC-5 goniometer with a rotating anode generator providing Mo$K\alpha$ radiation with a graphite monochromator, out to $(\sin\theta)/\lambda = 0.7$/A, with $-9 \le h \le 9$, $-15 \le k \le 15$, and $0 \le l \le 8$. The 212, $2\bar{1}2$, and 060 reflections were monitored as intensity and orientation standards every 150 reflections; their intensities varied by up to 1.5% from the mean. A total of 2138 symmetry-allowed reflections were measured, of which 1504 were observed at $I \ge 2\sigma_I$. Unit-cell parameters were determined from the positions of 24 centered reflections in the range $31 \le 2\theta \le 39$. Absorption corrections were made with the Agnost program supplied as part of the diffractometer con-

* Present address: Bayerisches Geoinstitut, Postfach 10 12 51, W-8580 Bayreuth, Germany.

0003–004X/92/0910–0937$02.00

TABLE 1. Refinement conditions and refined parameters of cubanite at several pressures

		0 GPa in air	0 GPa in cell	1.7 GPa	3.6 GPa
Number of observations ($I > 2\sigma$)		479	180	166	165
R (%)		2.2	5.0	4.6	4.6
Weighted R (%)		2.9	7.9	8.3	7.6
Extinction, r^* ($\times 10^5$)		4.0(2)	5.4(5)	5.2(5)	0.6(1)
Atom	Parameter				
Cu	x	0.5836(1)	0.5827(12)	0.5834(13)	0.5831(12)
	y	¼	¼	¼	¼
	z	0.1227(1)	0.1209(7)	0.1168(7)	0.1114(7)
	B	1.49(1)	1.90(10)	2.06(9)	1.67(9)
Fe	x	0.41479(8)	0.4124(9)	0.4118(9)	0.4066(9)
	y	0.41293(4)	0.4124(3)	0.4127(2)	0.4132(2)
	z	0.63664(7)	0.6377(5)	0.6335(4)	0.6298(5)
	B	0.92(1)	1.26(8)	1.50(7)	1.32(7)
S1	x	0.5857(4)	0.596(6)	0.596(6)	0.611(5)
	y	¼	¼	¼	¼
	z	0.7577(2)	0.7595(12)	0.7556(10)	0.7503(11)
	B	0.96(3)	1.55(28)	1.43(26)	1.67(34)
S2	x	0.4116(2)	0.4080(30)	0.4124(34)	0.4245(29)
	y	0.41545(8)	0.4158(8)	0.4151(7)	0.4146(8)
	z	0.26703(11)	0.2657(7)	0.2621(7)	0.2564(7)
	B	0.99(2)	1.42(15)	1.66(15)	1.19(16)

trol software. Equivalent reflections were averaged in point group *mmm* to give 681 unique reflections, of which 479 with $I \geq 2\sigma_I$ were used for structure solution and refinement.

High-pressure experiments

The single crystal (30 × 60 × 100) μm studied at room pressure was mounted in a diamond-anvil cell designed for single-crystal X-ray diffraction studies (Hazen and Finger, 1982). An Inconel 750X gasket with a hole 0.35 mm in diameter was centered over one 1.0-mm diamond anvil, and the crystal was centered on the face with a small dot of the alcohol-insoluble fraction of Vaseline petroleum jelly. We used a mixture of 4:1 methanol to ethanol as the hydrostatic pressure medium, and several 10 μm fragments of ruby were sprinkled near the crystals for internal pressure calibration. Special care was taken to ensure that a clearance of 0.1 mm was maintained between the crystals and gasket wall. This precaution prevents significant X-ray shadowing of the crystal by the gasket wall.

All high-pressure X-ray data were obtained on a Huber automated four-circle diffractometer with graphite monochromatized Mo$K\alpha$ radiation. Unit-cell parameters for the crystal were measured at six pressures to 3.6 GPa with the procedure of King and Finger (1979), whereby several reflections are measured in eight equivalent orientations. This procedure minimizes errors associated with crystal centering and diffractometer alignment. All refinements, furthermore, relied on reflections within a relatively narrow 2θ range, from 18 to 33°, in order to reduce systematic errors associated with measuring lattice parameters at different 2θ ranges (Swanson et al., 1985).

In an effort to improve pressure calibration, the pressure cell was opened, and the cubanite crystal was remounted with a cleavage fragment of calcium fluoride 100 × 100 × 10 μm thick as an additional pressure standard, along with ruby chips. The 2θ values of fluorite 220, 202, and $0\bar{2}2$ reflections provide a sensitive internal pressure standard (Hazen and Finger, 1981). Unit-cell parameters were measured at an additional 12 pressures to 3.68 GPa, and pressures were measured by both ruby and calcium fluoride methods. At several pressures only calcium fluoride pressures were obtained, owing to the failure of the laser in the ruby calibration system.

When comparing unit-cell parameters at several pressures, it is important to employ the same set of reflections for each measurement. Cell refinements at all pressures were determined with the same set of eight reflections: $\bar{4}40$, 042, 033, 403, $4\bar{4}2$, $\bar{4}42$, $\bar{4}60$, and $\bar{2}70$ (the eight Friedel pairs are also included by the eight-reflection centering routine).

Intensity data were obtained for the cubanite at 0.0, 1.76, and 3.59 GPa, prior to the inclusion of the calcium fluoride internal pressure standard. The rectangular cleavage fragment of cubanite was mounted with the a axis approximately perpendicular to the flat diamond fac-

TABLE 2. Anisotropic thermal parameters ($\times 10^3$) for cubanite at room conditions

Atom	β_{11}	β_{22}	β_{33}	β_{12}	β_{13}	β_{23}
Cu	9.51(15)	3.25(5)	8.29(14)	0	0	0
Fe	5.53(11)	1.74(3)	6.27(10)	−0.06(6)	0.37(10)	0.10(5)
S1	5.86(44)	1.79(9)	6.63(26)	0	0	0
S2	6.17(25)	1.98(6)	6.18(15)	−0.06(19)	−0.43(17)	−0.51(8)

TABLE 3. Cubanite anisotropic thermal ellipsoids at room conditions

Atom	Axis	Rms amplitude (Å)	Angle with respect to		
			a	*b*	*c*
Cu	1	0.127(1)	90	90	0
	2	0.142(1)	0	90	90
	3	0.142(1)	90	0	90
Fe	1	0.103(1)	65(10)	34(11)	111(6)
	2	0.107(1)	137(10)	57(12)	66(7)
	3	0.113(1)	57(6)	85(6)	33(6)
S1	1	0.106(3)	90	0	90
	2	0.111(4)	0	90	90
	3	0.114(2)	90	90	0
S2	1	0.101(2)	74(9)	51(5)	43(5)
	2	0.114(3)	151(15)	62(13)	95(17)
	3	0.119(2)	113(19)	128(11)	47(7)

es. All accessible reflections [approximately 30% of reflections to $(\sin\theta)/\lambda \leq 0.7$] were collected with ω step scans of 0.025° for 4 s per step. The fixed-ϕ mode of data collection (Finger and King, 1978) was used to optimize reflection accessibility and minimize attenuation by the diamond and Be components of the pressure cell. Data were corrected for Lorentz and polarization effects, crystal absorption, and X-ray absorption by the diamond cell (Hazen and Finger, 1982).

RESULTS

Room-pressure refinement

Refinement conditions, refined isotropic extinction coefficient (Zachariasen, 1967), refined positional parameters, and equivalent isotropic temperature factors are listed in Table 1. Refined anisotropic thermal parameters are in Table 2, corresponding magnitudes and orientations of vibration ellipsoids appear in Table 3, and tabulated calculated and observed structure factors are given in Tables 4A–4D.[1]

Single-crystal refinements of cubanite have been reported by Azaroff and Buerger (1955), Fleet (1970), and Szymanski (1974). The refined parameters agree most closely with the data of Szymanski (1974), who used a spherical crystal to eliminate systematic errors in the data due to absorption, extinction, and Renniger effects. The positional parameters agree to within 0.0004 in all cases. The vibration ellipsoids in the present data set are close to spherical (Table 2), in agreement with previous data. Interatomic distances and angles are given in Table 5; these also agree with the data of Szymanski (1974). In particular, our data show the same systematic pattern of Fe-S bond lengths, which supports the presence of an Fe-Fe repulsion force, in contrast to the Fe-Fe attraction force suggested by Fleet (1970).

[1] A copy of Table 4 may be ordered as Document AM-92-506 from the Business Office, Mineralogical Society of America, 1130 Seventeenth Street NW, Suite 330, Washington, DC 20036, U.S.A. Please remit $5.00 in advance for the microfiche.

TABLE 5. Selected interatomic distances and angles for cubanite at several pressures

Parameter	0 GPa in air	0 GPa in cell	1.7 GPa	3.6 GPa
Cu tetrahedron				
Cu-S1	2.271(1)	2.250(1)	2.229(9)	2.209(10)
Cu-S1	2.295(3)	2.249(35)	2.23(4)	2.12(3)
Cu-S2 [2]	2.327(1)	2.338(13)	2.306(13)	2.242(12)
Mean Cu-S	2.305(1)	2.294(1)	2.268(5)	2.203(5)
S1-Cu-S1	111.1(1)	110.4(7)	110.5(8)	109.0(7)
S1-Cu-S2 [2]	107.6(1)	107.3(6)	106.9(7)	104.7(6)
S1-Cu-S2 [2]	112.9(1)	113.7(6)	113.9(7)	115.4(5)
S2-Cu-S2	104.3(1)	103.8(7)	104.2(8)	106.6(7)
Fe tetrahedron				
Fe-S1	2.249(2)	2.285(19)	2.276(21)	2.324(19)
Fe-S2	2.259(1)	2.216(19)	2.225(21)	2.238(18)
Fe-S2	2.290(1)	2.311(11)	2.298(12)	2.272(11)
Fe-S2	2.300(1)	2.314(6)	2.291(5)	2.280(5)
Mean Fe-S	2.275(1)	2.282(7)	2.273(8)	2.279(7)
S1-Fe-S2	110.0(1)	107.7(4)	107.6(4)	106.0(4)
S1-Fe-S2	110.3(1)	112.2(9)	112.1(9)	114.8(8)
S1-Fe-S2	110.4(1)	110.5(5)	109.8(6)	107.1(6)
S2-Fe-S2	104.8(1)	104.7(3)	105.7(3)	106.0(3)
S2-Fe-S2	110.5(1)	110.3(4)	110.9(5)	113.1(4)
S2-Fe-S2	110.6(1)	111.2(4)	110.4(4)	109.3(4)
S1 tetrahedron				
S1-Cu	2.271(1)	2.250(10)	2.229(9)	2.209(10)
S1-Cu	2.295(3)	2.249(35)	2.23(4)	2.12(3)
S1-Fe [2]	2.249(2)	2.285(19)	2.276(21)	2.324(19)
Cu-S1-Cu	111.8(1)	114.7(13)	114.7(14)	118.2(12)
Cu-S1-Fe [2]	109.4(1)	108.2(8)	108.2(8)	105.7(8)
Cu-S1-Fe [2]	109.5(1)	110.6(6)	110.6(7)	112.6(5)
Fe-S1-Fe	107.1(1)	104.1(12)	104.0(14)	100.2(11)
S2 tetrahedron				
S2-Cu	2.327(1)	2.338(13)	2.306(13)	2.242(12)
S2-Fe	2.259(1)	2.216(19)	2.225(21)	2.238(18)
S2-Fe	2.290(1)	2.311(11)	2.298(12)	2.272(11)
S2-Fe	2.300(1)	2.314(6)	2.291(5)	2.280(5)
Cu-S2-Fe	107.3(1)	107.4(5)	107.3(5)	106.2(5)
Cu-S2-Fe	111.8(1)	111.5(5)	112.4(5)	114.3(5)
Cu-S2-Fe	121.6(1)	120.5(8)	121.8(10)	124.9(9)
Fe-S2-Fe	124.1(1)	125.2(6)	124.6(6)	123.6(6)
Fe-S2-Fe	111.5(1)	111.7(7)	110.8(8)	107.3(6)
Fe-S2-Fe	75.2(1)	75.4(3)	74.3(3)	74.0(3)
Fe-Fe	2.800(1)	2.827(7)	2.773(7)	2.738(7)

Note: Bracketed numbers represent multiplicity of bond distances or angles.

Linear compressibilities

The variations in the lattice parameters of cubanite as a function of pressure are listed in Table 6 and illustrated in Figure 1. The cell parameters can be fitted to straight lines within the resolution of the data set:

$$a = 6.458(1) - 0.0328(3)P \quad (1)$$

$$b = 11.104(1) - 0.0527(6)P \quad (2)$$

and

$$c = 6.220(1) - 0.0354(2)P. \quad (3)$$

The linear compressibilities are as follows:

$$\beta_a = 5.13(5) \times 10^{-3}/\text{GPa} \quad (4)$$

$$\beta_b = 4.79(5) \times 10^{-3}/\text{GPa} \quad (5)$$

and

$$\beta_c = 5.75(4) \times 10^{-3}/\text{GPa}. \quad (6)$$

TABLE 6. Cubanite unit-cell parameters vs. pressure

P (GPa)					
Ruby	CaF_2	a (Å)	b (Å)	c (Å)	V (Å³)
0	0	6.460(4)	11.058(2)	6.225(8)	444.7(11)
0	0	6.456(7)	11.108(5)	6.224(2)	446.3(5)
0	0	6.451(8)	11.101(3)	6.222(3)	445.6(6)
0	0	6.459(5)	11.104(2)	6.220(2)	446.1(3)
0.04	—	6.455(6)	11.102(2)	6.226(2)	446.2(4)
0.38	0.25	6.446(1)	11.082(4)	6.207(1)	443.4(2)
—	0.26	6.451(6)	11.096(6)	6.215(3)	444.9(4)
1.07	0.87	6.427(1)	11.051(5)	6.185(1)	439.3(2)
—	0.87	6.432(2)	11.064(2)	6.193(1)	440.7(1)
1.17	—	6.425(7)	11.043(2)	6.184(2)	438.8(5)
1.36	1.2	6.420(1)	11.032(4)	6.177(1)	437.5(2)
1.76	—	6.413(6)	11.019(2)	6.167(2)	435.8(4)
1.76	—	6.398(8)	10.996(2)	6.150(2)	432.7(5)
1.78	1.51	6.401(1)	11.015(4)	6.154(1)	433.9(2)
1.99	1.82	6.393(1)	11.016(22)	6.147(1)	432.9(9)
2.32	—	6.391(5)	10.988(2)	6.145(2)	431.5(3)
—	2.34	6.381(2)	10.985(2)	6.138(1)	430.2(2)
—	2.88	6.364(1)	10.948(4)	6.113(1)	425.9(2)
3.08	—	6.359(7)	10.937(2)	6.109(2)	424.9(5)
3.22	3.28	6.359(1)	10.942(4)	6.108(1)	425.0(2)
—	3.35	6.356(4)	10.929(4)	6.107(2)	424.2(3)
—	3.46	6.353(4)	10.915(5)	6.098(2)	422.9(3)
3.59	—	6.344(4)	10.919(2)	6.098(1)	422.4(3)
3.65	3.68	6.331(1)	10.892(6)	6.079(2)	419.2(3)

The relative compressibilities are illustrated in Figure 2. The compressibilities of the a and b axes are similar, whereas the c axis is approximately 15% more compressible. This difference in relative compressibilities is easily understood in terms of the crystal structure. The approximately hexagonal closest packing arrangement of S atoms in layers perpendicular to the c axis results in a larger compressibility of the c axis.

Bulk modulus

The V/V_0 compression data were fitted to a third-order Birch-Murnaghan equation of state Taylor expansion of energy in terms of Eulerian finite strain (Birch, 1952, 1978):

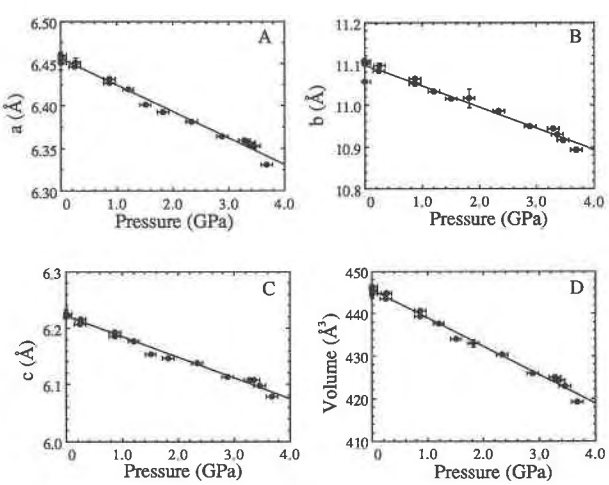

Fig. 1. Compression of cubanite at high pressure for (**A**) a axis; (**B**) b axis; (**C**) c axis; and (**D**) unit-cell volume. The solid lines represent least-squares fits to the data.

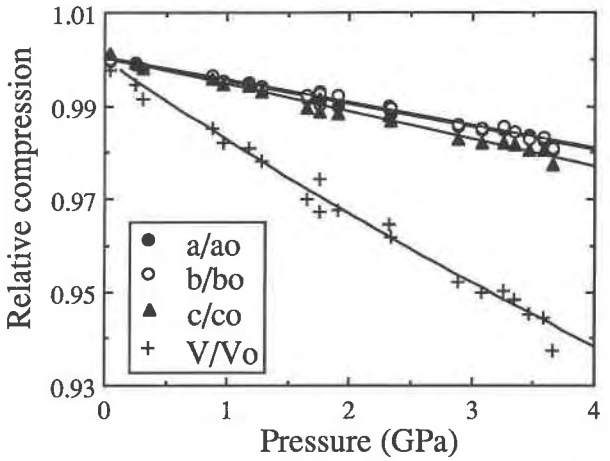

Fig. 2. Relative compression of cubanite at high pressure. The solid lines through the data for a/a_0, b/b_0, and c/c_0 are linear least-squares fits to the data, whereas the solid line through the V/V_0 data is a Birch-Murnaghan equation of state with $K = 55.3$ GPa and $K_0' = 4$.

$$P = 3f(1 + 2f^{5/2}[1 - 3f/2(4 - K_0')] \quad (7)$$

where the Eulerian finite strain is given by

$$f = \tfrac{1}{2}[(V/V_0)^{-2/3} - 1]. \quad (8)$$

A least-squares fit of the cubanite data to a third-order equation of state gives the values $K = 56.8 \pm 3.8$ GPa, $K_0' = 2.2 \pm 1.0$, and $V_0 = 447.3 \pm 0.6$ Å³, whereas a second-order fit of the data ($K_0' = 4$) gives a bulk modulus of $K = 55.3 \pm 1.7$ GPa. V_0 was considered a fit parameter because "0 GPa" values measured before and after high-pressure experiments are actually made at some pressure between 0.0 and 0.1 GPa. The reason is that pressure fluid must be retained in the cell; otherwise the surface tension of expanding air bubbles in the pressure chamber can push crystals out of orientation. Our fitted value of V_0 is in excellent agreement with previous data (Fleet, 1970; Szymanski, 1974). The compression data are illustrated in Figure 2, where the theoretical curve corresponding to a Birch-Murnaghan equation of state with parameters $K = 55.3$ GPa and $K_0' = 4$ is included for comparison.

The uncertainty of the bulk modulus is best illustrated in a plot of normalized pressure (F) vs. finite strain (f). The normalized pressure can be written

$$F = P/[3f(1 + 2f)^{5/2}] \quad (9)$$

and so Equation 4 becomes

$$F = K_0[1 - 3/2f(4 - K_0')] \quad (10)$$

(Birch, 1978; see also Jeanloz, 1981). The compression data are illustrated in a plot of F vs. f in Figure 3. The horizontal line corresponds to $K_0' = 4$, and the degree to which K is dependent on the value of K_0' can be clearly seen. It is evident that the simplifying assumption $K_0' = 4$ (horizontal line) is consistent with the data, and in view

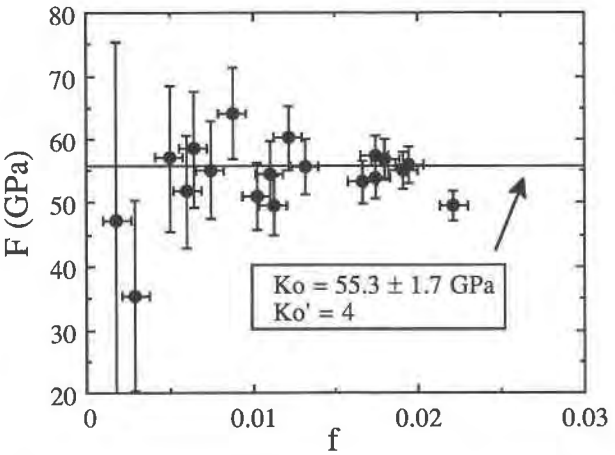

Fig. 3. Compression data of cubanite plotted on an F (normalized pressure) vs. f (finite strain) plot. The line represents the best fit with a constrained $K_0' = 4$ and a fitted value of $V_0 = 447.3$ Å^3.

of the uncertainties we feel that the data do not support a third-order fit (K_0' unconstrained).

High-pressure structures

Selected interatomic distances and angles are given in Table 5, unit-cell parameters appear in Table 6, and polyhedral volumes and distortion indices for the four atoms (all of which are tetrahedrally coordinated) are in Table 7. When describing the changes of a crystal structure resulting from high pressure, it is important to use a reference room-pressure refinement based on intensity data obtained using the crystal in the diamond cell. Significant differences are typically observed, particularly in thermal parameters, between refined parameters for room-pressure crystals in air and in the pressure cell (Tables 1, 5). Systematic errors arise in the diamond cell data from absorption complexities and the limited access to reciprocal space. In the case of cubanite, all atomic coordinates agree within about 2 esd, but the in-cell thermal parameters average almost 50% greater than those measured in air.

TABLE 7. Polyhedral volumes and distortion indices* of cubanite vs. pressure

	0 GPa in air	0 GPa in cell	1.7 GPa	3.6 GPa
Cu tetrahedron				
Volume (Å^3)	6.258(7)	6.16(8)	5.94(8)	5.42(7)
Quad. elong.	1.003(1)	1.004(18)	1.004(11)	1.008(10)
Angle var.	12.0	15.9	16.6	25.2
Fe tetrahedron				
Volume (Å^3)	6.027(5)	6.08(6)	6.01(6)	6.04(5)
Quad. elong.	1.001(1)	1.002(8)	1.001(8)	1.004(7)
Angle var.	5.4	7.8	5.8	14.4
S1 tetrahedron				
Volume (Å^3)	5.963(2)	5.96(5)	5.84(5)	5.75(4)
Quad. elong.	1.001(1)	1.003(19)	1.003(18)	1.009(16)
Angle var.	2.4	12.3	12.8	41.9
S2 tetrahedron				
Volume (Å^3)	5.408(3)	5.43(3)	5.27(3)	5.07(3)
Quad. elong.	1.095(1)	1.094(8)	1.100(29)	1.107(8)
Angle var.	309.9	308.3	325.1	346.5

* Robinson et al. (1971).

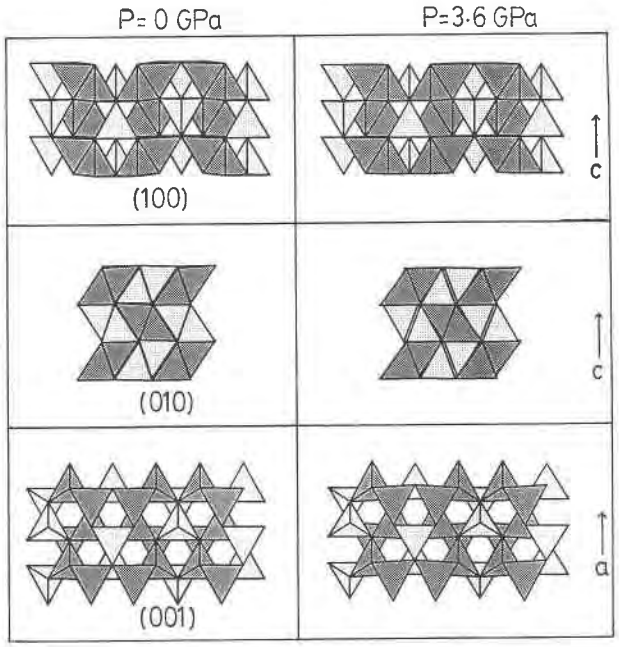

Fig. 4. Polyhedral representation of the (100), (010), and (001) layers of cubanite at 0 and 3.6 GPa. The Fe tetrahedra are shaded in dark gray and the Cu tetrahedra are shaded in light gray. The orientation of each section is shown by an arrow indicating either the c or a axis.

The principal response of the cubanite crystal structure to pressure is a dramatic shortening of Cu-S bonds. From Table 5 the mean Cu-S distance contracts between 0 and 3.6 GPa from 2.305 to 2.203 Å (4.4%). This change corresponds to a 13.4% reduction in the volume of the Cu tetrahedron (Table 7). In contrast, the mean Fe-S distance remains virtually unchanged at 2.279 Å, whereas the Fe-Fe distance is shortened from 2.800 to 2.738 Å (2.2%). The effect on the crystal structure is a change in bond angles to accommodate the shrinking Cu tetrahedra. Figure 4 illustrates a polyhedral view of the crystal structure at 0 and 3.6 GPa. The (100) layer illustrates the smaller Cu tetrahedron at 3.6 GPa accompanied by a change in Cu-S-Fe bond angles, resulting in a relative tilting of the tetrahedra. The degree of tilting is best seen in the (010) layer, where the smaller size of the Cu tetrahedra relative to Fe is evident from the increase in the size of the gaps between tetrahedra. The (001) layer illustrates the closing of Fe-S-Fe angles to accommodate the smaller Cu tetrahedra at 3.6 GPa.

DISCUSSION

Comparison of cubanite bulk modulus with other sulfides

The compression of cubanite appears anomalous because of the large difference in the relative compressibilities of the cation tetrahedra, and it is useful to compare

TABLE 8. Bulk moduli of some sulfide compounds

Compound	K_0 (GPa)	K_0'	Reference
ZnS (wurtzite)	77(8)	—	Simmons and Wang (1971)
FeS_2	148	5.5	Clendenen and Drickamer (1966)
	147.9(5)	4	Jephcoat et al. (1983)
	118(4)	4	Will et al. (1984)
FeS*	82(7)	4	King and Prewitt (1982)
CoS_2	115(4)	4	Will et al. (1984)
CuS*	54(1)	4	Takéuchi et al. (1985)

* Volume data from reference were fitted to second-order Birch-Murnaghan equation of state.

the derived bulk modulus with data from other sulfide compounds. Table 8 lists values obtained from the literature and demonstrates that the bulk modulus of cubanite is low compared to similar sulfides. The closest structural analogue to cubanite is ZnS in the wurtzite structure, which has a bulk modulus that is 40% greater than that of cubanite. The highest axial compressibility of cubanite is along the c axis, however, which is perpendicular to the wurtzite layers; therefore, a direct comparison of the structure compressibilities is probably not appropriate. The compressibility of cubanite is determined primarily by the compressibility of Cu^{1+} tetrahedra, and one might therefore expect a similarity in the bulk moduli of copper sulfides. The bulk modulus of CuS determined from single-crystal compression experiments of Takéuchi et al. (1985) agrees very well with the bulk modulus of cubanite, although it should be noted that the structure of CuS consists of triangular CuS_3 groups as well as CuS_4 tetrahedra. The negligible compressibilities of the Fe-S bonds observed in cubanite are not duplicated in either of the iron sulfides FeS or FeS_2. In pyrite, FeS_2, the unit-cell translation length is twice the Fe-S_2 distance, so the bulk modulus directly reflects the reduction in cation-anion bond distance. High-pressure single-crystal refinements of King and Prewitt (1982) have shown that the Fe-S distance in FeS also shortens with pressure.

In order to quantify the comparison of the compressibilities of the different sulfides, it is useful to consider the individual cation polyhedra. Hazen and Finger (1979) showed that a relationship between bulk modulus and volume exists for a wide variety of cation coordination polyhedra, including sulfide compounds. They found the general relationship

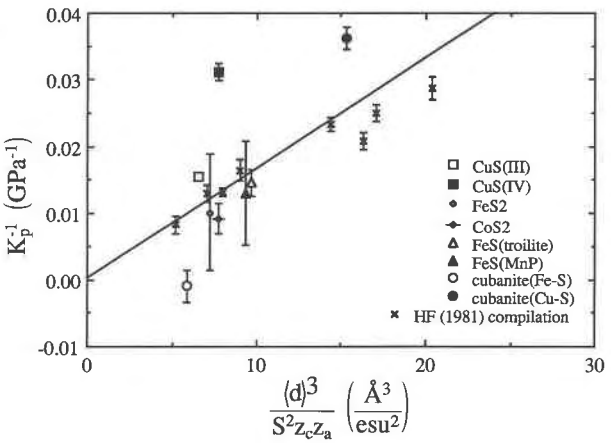

Fig. 5. Polyhedral bulk modulus data for some sulfides. Values from the previous compilation of Hazen and Finger (1981) are indicated by crosses, and the line indicates the general bulk modulus relationship $K_P d^3/S^2 z_c z_a = 750$ GPa Å^3.

$$K_P d^3/S^2 z_c z_a = 750 \text{ GPa Å}^3 \quad (11)$$

where K_P is the effective polyhedral bulk modulus, d is the cation-anion separation, S^2 is an empirical ionicity term, and z_c and z_a are the cation and anion formal charges, respectively. For sulfides, S^2 was determined to be 0.4. We have updated the compilation of Hazen and Finger (1979) with recent data from experiments on sulfides; the data are listed in Table 9 and plotted in Figure 5. Note that the slight expansion in the mean Fe-S distance with pressure (Table 5) results in a negative polyhedral bulk modulus for the Fe tetrahedron, a value inconsistent with the empirical Equation 11. From Table 9 it is evident that the data for FeS_2, CoS_2, FeS (troilite), and FeS (MnP type) are in good agreement with the relationship between bulk modulus and volume; however, the data for CuS and $CuFe_2S_3$ are not. From Figure 5 one sees that the Cu tetrahedra are more compressible than predicted by the relation, whereas the Fe tetrahedra of $CuFe_2S_3$ are much less compressible. As noted by Hazen and Finger (1979), deviations from relationship 11 tend to occur with significant covalence of chemical bonds, which may provide an explanation for the deviation of the Cu tetrahedra. In the case of the Fe tetrahedra, there is likely a large elec-

TABLE 9. Polyhedral bulk moduli for some sulfide compounds

Compound (polyhedron)	Structure type	$\langle d\rangle$ (Å)	K_P (GPa)	z_c	z_a	$\frac{K_P \langle d\rangle^3}{S^2 z_c z_a}$	Reference*
CuS (III)	covellite	2.191(1)	64(2)	2	2	420(5)	1
CuS (IV)	covellite	2.314(2)	32(1)	2	2	249(3)	1
FeS_2	pyrite	2.26(2)	99(86)	2	2	716(182)	2
CoS_2	pyrite	2.316(5)	108(28)	2	2	842(61)	2
FeS	troilite	2.492(2)	69(9)	2	2	663(23)	3
FeS	MnP	2.465(12)	77(46)	2	2	719(112)	3
$CuFe_2S_3$ (Fe-S)	cubanite	2.275(1)	−965(2239)	2.5	2	−5678(3842)	this work
$CuFe_2S_3$ (Cu-S)	cubanite	2.305(1)	28(1)	1	2	423(6)	this work

* References are (1) Takéuchi et al. (1985); (2) Will et al. (1984); (3) King and Prewitt (1982).

tronic contribution to the bulk modulus from the electron exchange occurring between Fe^{2+} and Fe^{3+}.

Alternatively, slight rotations and increased distortions of all cation tetrahedra (Fig. 4, Table 7), traits not observed in other sulfide structures studied at high pressure, may contribute to the lower than predicted compressibility of the Fe tetrahedra.

Effect of pressure on Fe^{2+}-Fe^{3+} electron exchange

The nature of the electron configuration of Fe is sensitive to cation-anion bond distances, since these determine the relative strength of electronic interactions. Intervalence charge transfer interactions have been observed to intensify in oxides and silicates at high pressure because of the contraction of metal-anion distances (see Burns, 1981, and references therein). The Fe-S distance in cubanite remains constant to 3.6 GPa, however, implying that the electron transfer process should be largely unchanged by the application of pressure.

It is interesting to speculate as to why Fe-S distances remain essentially constant in cubanite with increasing pressure. In FeS the Fe-S distance contracts from 2.492 to 2.452 Å between 0 and 3.3 GPa (King and Prewitt, 1982), and in FeS_2 the Fe-S distance shrinks from 2.26 to 2.23 Å between 0 and 3.8 GPa, so it seems likely that the behavior of $CuFe_2S_3$ is related to the electron transfer process. We can speculate that the Fe^{2+}-Fe^{3+} configuration in cubanite is unusually stable, and that, furthermore, the energy is lowest near 2.27 Å, the observed Fe-S distance in cubanite. Compression of the crystal structure, which is compatible with reduction in the Fe-S distance, results in a higher relative energy of the electron configuration, and therefore the Fe polyhedra resist compression. This behavior may be compared to vivianite, which exhibits localized Fe^{2+}-Fe^{3+} electrons across pairs of edge-shared octahedra. Initially, vivianite is easily oxidized, but it reaches a maximum level of Fe^{3+} concentration because of the stability of the Fe^{2+}-Fe^{3+} pair (McCammon and Burns, 1980).

Conclusions

We conclude the following based on our high-pressure crystallographic experiments between 0 and 3.7 GPa:

1. The c axis of cubanite is approximately 15% more compressible than the a or b axes, consistent with the approximate hexagonal closest packing of S atoms perpendicular to c.

2. The bulk modulus of cubanite is 55.3 ± 1.7 GPa with K_0' constrained to be 4.

3. The principal structural response to pressure is the shortening of Cu-S bonds by 4.4% between 0 and 3.6 GPa. The Fe-S distance remains essentially constant.

4. The compressibility of both Cu and Fe tetrahedra do not agree with the empirical relationship between bulk modulus and volume of Hazen and Finger (1979); we suggest this disagreement may be due to covalency of the Cu-S and Fe-S bonds, as well as contributions to compressibility by the electron transfer interactions of Fe^{2+}-Fe^{3+}.

5. We infer that the nature of electron transfer between Fe^{2+} and Fe^{3+} is essentially unchanged between 0 and 3.6 GPa on the basis of the constancy of Fe-S distances.

Acknowledgments

This work was performed while one of the authors (C.A.M.) was a visiting investigator at the Geophysical Laboratory. The visit was funded by the Natural Sciences and Engineering Research Council of Canada, through both the University Research Fellow Program and the Operating Grant Program. High-pressure crystallographic studies are supported at the Geophysical Laboratory by the Carnegie Institution of Washington, by NSF grant EAR-8916709, and by the NSF Center for High-Pressure Research.

References cited

Azaroff, L.V., and Buerger, M.J. (1955) Refinement of the structure of cubanite, $CuFe_2S_3$. American Mineralogist, 40, 213–225.

Birch, F. (1952) Elasticity and constitution of the Earth's interior. Journal of Geophysical Research, 57, 227–286.

——— (1978) Finite strain isotherm and velocities for single-crystal and polycrystalline NaCl at high pressures and 300 K. Journal of Geophysical Research, 83, 1257–1268.

Buerger, M.J. (1945) The crystal structure of cubanite, $CuFe_2S_3$, and the coordination of ferromagnetic iron. Journal of the American Chemical Society, 67, 2056.

——— (1947) The crystal structure of cubanite. American Mineralogist, 32, 415–425.

Burns, R.G. (1981) Electronic spectra of minerals at high pressure: How the mantle excites electrons. In W. Schreyer, Ed., High-pressure researches in geoscience, p. 223–246. E. Schweizerbart'sche Verlagsbuchhandlung, Stuttgart.

Clendenen, R.L., and Drickamer, H.G. (1966) Lattice parameters of nine oxides and sulfides as a function of pressure. Journal of Chemical Physics, 44, 4223–4228.

Finger, L.W., and King, H.E. (1978) A revised method of operation of the single-crystal diamond anvil cell and the refinement of the structure of NaCl at 32 kbar. American Mineralogist, 63, 337–342.

Fleet, M.E. (1970) Refinement of the crystal structure of cubanite and polymorphism of $CuFe_2S_3$. Zeitscrift für Kristallographie, 132, 276–287.

Goodenough, J.B. (1980) Structural chemistry of iron sulfides. Materials Research Bulletin, 13, 1305–1314.

Greenwood, N.N., Whitfield, H.J. (1968) Mössbauer effect studies on cubanite ($CuFe_2S_3$) and related iron sulfides. Journal of the Chemical Society (London) A, 1697–1699.

Hazen, R.M., and Finger, L.W. (1979) Bulk modulus-volume relationship for cation-anion polyhedra. Journal of Geophysical Research, 84, 6723–6728.

——— (1981) Calcium fluoride as an internal pressure standard in high-pressure/high-temperature crystallography. Journal of Applied Crystallography, 14, 234–236.

——— (1982) Comparative crystal chemistry. Wiley, New York.

Imbert, P., and Wintenberger, M. (1967) Études des propriétés magnétiques et des spectres d'absorption par effet Mössbauer de la cubanite et de la sternbergite. Bulletin de la Société Français de Minéralogie et de Cristallographie, 90, 299–303.

Jeanloz, R. (1981) Finite-strain equation of state for high-pressure phases. Geophysical Research Letters, 8, 1219–1222.

Jephcoat, A.P., Mao, H.K., and Bell, P.M. (1983) Pyrite: Hydrostatic compression to 40 GPa. Eos, 64, 847.

King, H.E., and Finger, L.W. (1979) Diffracted beam crystal centering and its application to high-pressure crystallography. Journal of Applied Crystallography, 12, 374–378.

King, H.E., and Prewitt, C.T. (1982) High-pressure and high-temperature polymorphism of iron sulfide (FeS). Acta Crystallographica, B38, 1877–1887.

McCammon, C.A., and Burns, R.G. (1980) The oxidation mechanism of vivianite as studied by Mössbauer spectroscopy. American Mineralogist, 65, 361–366.

Robinson, K., Gibbs, G.V., and Ribbe, P.H. (1971) Quadratic elongation: A quantitative measure of distortion in coordination polyhedra. Science, 172, 567–570.

Simmons, G., and Wang, H. (1971) Single crystal elastic constants. Massachusetts Institute of Technology Press, Cambridge, Massachusetts.

Sleight, A.W., and Gillson, J.L. (1973) Electrical resistivity of cubanite: $CuFe_2S_3$. Journal of Solid State Chemistry, 8, 29–30.

Swanson, D.K., Weidner, D.J., Prewitt, C.T., and Kandelin, J.J. (1985) Single-crystal compression of γ-Mg_2SiO_4. Eos, 66, 370.

Szymanski, J.T. (1974) A refinement of the structure of cubanite, $CuFe_2S_3$. Zeitschrift für Kristallographie, 140, 218–239.

Takéuchi, Y., Kudoh, Y., and Sato, G. (1985) The crystal structure of covellite CuS under high pressure up to 33 kbar. Zeitschrift für Kristallographie, 173, 119–128.

Will, G., Lauterjung, J., Schmitz, H., and Hinze, E. (1984) The bulk moduli of 3d-transition element pyrites measured with synchrotron radiation in a new belt type apparatus. Materials Research Society Symposium Proceedings, 22, 49–52.

Wintenberger, M., Lambert-Andron, B., and Roudaut, E. (1974) Détermination de la structure magnétique de la cubanite par diffraction neutronique sur un monocristal. Physica Status Solidi, A26, 147–154.

Zachariasen, W.H. (1967) A general theory of X-ray diffraction in crystals. Acta Crystallographica, 23, 558–564.

Manuscript received December 13, 1991
Manuscript accepted May 21, 1992